Int. J. Electrochem. Sci., 16 **(2021)** Article ID: 210918, doi: 10.20964/2021.09.29

International Journal of
ELECTROCHEMICAL
SCIENCE
www.electrochemsci.org

Pt supported on C-TiO_2 and C-ZrO_2 Composite Materials and Their Evaluation in the Anodic Oxidation of Ethanol

M. Castro-Gómez[1], A. Gutiérrez-Alejandre[1], M. Aguilar-Franco[3], L. C. Ordoñez[2,]*

[1] UNICAT, Departamento de Ingeniería Química, Facultad de Química, UNAM, Ciudad Universitaria, Ciudad de México (04510), Mexico.
[2] Unidad de Energía Renovable, Centro de Investigación Científica de Yucatán, Parque Científico Tecnológico de Yucatán, Carretera Sierra Papacal – Chuburná Puerto, km 5. Sierra Papacal, Yucatán (97302), Mexico.
[3] Instituto de Física, Universidad Nacional Autónoma de México, A. P. 20-364, México, D.F., Mexico.
[*]E-mail: lcol@cicy.mx

Received: 18 May 2021 / *Accepted:* 1 July 2021 / *Published:* 10 August 2021

C-TiO_2 and C-ZrO_2 composite materials were prepared with different metal oxide contents (C-TiX and C-ZrX series with X = 5, 23 and 50 wt. % TiO_2 or ZrO_2, respectively) to modify their surface acidity and to evaluate their effects on the Pt catalyst activity for the oxidation of ethanol in acid medium. Pt catalysts were synthesized via incipient impregnation. The supports were characterized by X-ray diffraction (XRD) and UV-Vis diffuse reflectance spectroscopy (UV-Vis DRS). The electrical conductivity was analyzed in a two-electrode cell. The surface acidity of the supports was determined by potentiometric titration with n-butylamine. The electrocatalytic activity for ethanol oxidation was evaluated through cyclic voltammetry and electrochemical impedance spectroscopy. The XRD results showed that the metal oxides were not introduced into the carbon structure. The UV-Vis-DRS and conductivity results showed that the electronic properties of the C-TiX and C-ZrX supports were modified by the metal oxide content. TiO_2 and ZrO_2 incorporation into the support formulation decreased the total surface acidity strength but increased the concentration of acid sites, which had a positive effect on the electrocatalytic activity observed as a reduction in the charge-transfer resistance. The Pt/C-Ti23 and Pt/C-Zr23 catalysts were the most active of the tested composites.

Keywords: Pt/C-TiO_2, Pt/C-ZrO_2, ethanol electro-oxidation, support acidity, DAFC.

1. INTRODUCTION

Interest in the development of direct ethanol fuel cells (DEFCs) as a power supply has grown in recent decades because ethanol can be easily handled and transported using the current infrastructure for the use of fossil fuels [1]. Furthermore, this low-molecular-weight alcohol can be produced by

fermenting raw materials rich in sugars and can even be produced sustainably if organic waste is used. Nevertheless, DEFCs present problems that currently prevent them from being scaled up to a commercial level: ethanol crossover from the anode compartment to the cathode generates mixed potentials and cell depolarization, and the poisoning of platinum catalytic sites due to the presence of intermediate species from the ethanol electro-oxidation reaction (EOR). The incorporation of metal oxides such as TiO_2 and ZrO_2 has been proposed as an alternative for increasing the activity of Pt/C catalysts for the EOR [2-6]. The presence of these oxides improves the mechanical and textural properties of the carbon support [7]. In $PtRuTiO_2$/C catalyst, the electronic properties of Pt change due to the strong interaction between Pt and TiO_2, which reduces the adsorption strength of CH_3OH and the intermediate species (such as CO) on the Pt active sites and facilitates their oxidation [8, 9]. In addition, the presence of TiO_2 promotes an increase in the electrochemically active area of platinum and, consequently, in its methanol oxidation activity. Similarly, if TiO_2 is used in the cathode catalyst, it increases the oxygen reduction activity [10, 11]. In TiO_2-C composite supports, TiO_2 enhances the support resistance to corrosion by reducing the Pt-C contact area [6, 7, 12]. Shim [13] found that the incorporation of TiO_2 and WO_3 oxides onto the surface of a commercial Pt/C catalyst increased the overall efficiency of an H_2-O_2 fuel cell and that varying the TiO_2 content in the Pt/C-TiO_2 catalyst reduced the oxygen and hydrogen adsorption strength on the Pt surface. These researchers also concluded that titanium oxide content increases the active area. Additionally, Xiong [14] reported that both the synthesis method and the thermal treatment influence the catalytic activity of Pt/C-TiO_2 catalysts. Better performance was obtained with thermal treatment at 500 °C, while thermal treatment at 900 °C produced an increase in the Pt particle size, reducing the electrochemical performance of the direct methanol fuel cell. Bauer [2] reported that coating the carbon support with titanium dioxide improves Pt particle dispersion and generally improves catalyst stability. Ru@Pt/C-TiO_2 catalysts evaluated in the methanol oxidation reaction showed a higher tolerance to the intermediary species such as CO than did Pt/C due to the strong electronic interaction between Pt and TiO_2

Additionally, when incorporating ZrO_2 into Pt/C catalysts, the catalytic activity increases by improving the overall acidity at the reaction interface [6]. The incorporation of ZrO_2 into Pt catalysts supported on carbon nanotubes causes an increase in the EOR activity as a result of a) the presence of oxygen vacancies in ZrO_2, which favor the transport of protons at the electrochemically active interface and the dissociation of water, thereby generating surface –OH groups; and b) a bifunctional mechanism, in which the –OH groups present on the ZrO_2 surface favor the oxidation of CO adsorbed on the Pt sites to generate CO_2. In addition, the catalytic activity for the EOR can be optimized by modifying the Pt:ZrO_2 ratio, which should be no more than 1:1 because of the low electrical conductivity of this oxide [15, 16]. Bai [5] compared the EOR catalytic activity of a Pt-ZrO_2/C catalyst in an alkaline medium to that of Pt/C and found that there is no atomic interaction between Pt and ZrO_2. The catalyst with a 1:1 Pt:ZrO_2 molar ratio exhibited a higher catalytic activity and a lower resistance to charge transfer than did the Pt/C catalyst, indicating that Pt-Zr/C catalysts are a viable alternative for the electro-oxidation of ethanol. Song [15] reported that the incorporation of ZrO_2 into carbon nanotubes used to support Pt catalysts increases the catalytic activity for the oxidation of both methanol and ethanol. It has also been observed that depositing ZrO_2 on solid alkaline membranes [17] facilitates the ionic conductivity of the membrane for use in alkaline fuel cells exceptionally well.

This work studies how the Pt catalytic activity for the ethanol electro-oxidation reaction is affected by varying the carbon support surface properties (surface acidity, specific area, and structure) by incorporating TiO_2 or ZrO_2 at variable loadings. With this objective, the surface and bulk properties of the supports were studied by X-ray diffraction (XRD), UV-Vis diffuse reflectance spectroscopy and potentiometric titration with n-butylamine. The catalyst activity was evaluated by cyclic voltammetry and electrochemical impedance spectroscopy.

2. EXPERIMENTAL

2.1 Synthesis of the supports

C-TiO_2 and C-ZrO_2 supports with different metal oxide contents (C-TiX and C-ZrX series with X = 5, 23 and 50 wt. % TiO_2 or ZrO_2, respectively) were prepared according to the method described by Wang [8]. The required amount of Vulcan XC72R® carbon was dispersed in 80 mL of ethanol to achieve the desired weight percentage using an ultrasonic bath for 20 minutes. For the C-TiX series, the required amount of titanium butoxide ($Ti(OBu)_4$) was added dropwise to the system while continuously stirring at room temperature and under a N_2 atmosphere. Zirconium butoxide ($Zr(OBu)_4$) was used as the ZrO_2 precursor in the C-ZrX series. After 4 h, an ethanol-water mixture was added dropwise, and the system was stirred continuously for 12 h. After this time, the materials were recovered by filtration and washed several times with type I deionized water. Then, the materials were dried at 100 ºC for 12 h. Finally, a thermal treatment was performed under a N_2 atmosphere for 2 h at 450 ºC.

2.2 Synthesis of the catalysts

The Pt/C-TiX and Pt/C-ZrX catalysts were prepared by the incipient impregnation method. The support was impregnated with the required amount of a chloroplatinic acid (H_2PtCl_6) solution to achieve 20 wt% Pt. Next, the sample was aged for 24 h at room temperature and then dispersed in 40 mL of water and 100 mL of 0.5 M $NaBH_4$ was added dropwise while continuosly stirring for 1 h. The catalyst was recovered by filtration and washed several times with type I deionized water. Finally, the catalyst was dried at 100 °C for 24 h.

2.3 Physicochemical characterization

The X-ray diffractograms were collected using a Siemens D500 diffractometer equipped with a copper anode and CuKα radiation with λ = 0.15406 nm. The equipment was operated at a voltage of 40 kV and a current of 30 mA. The crystalline structures were refined using the Rietveld method implemented in the TOPAS code, academic version 4.1 [18]. The crystallite size and morphology were modeled in reciprocal space with symmetrized harmonic expansion [19]. The lattice deformations were assumed to be anisotropic and were modeled with a multidimensional distribution of lattice metrics

[20]. The background model was a polynomial function that, in addition to the constant, linear, quadratic, and cubic terms in 2θ, also included the terms (1/2θ) and (1/2θ)2. The standard deviations, given in parentheses in the text, show the variation in the last digit of a number; when the values correspond to the Rietveld refined parameters, they are not estimates of the probable error in the analysis as a whole but only of the minimum possible errors that are probable based on a normal distribution [21].

UV-Vis diffuse reflectance spectroscopy experiments at room temperature were performed using a UV-Vis-NIR Varian Cary 500 spectrophotometer.

The N_2 physisorption tests were performed at 77 K using an Autosorb-1 instrument from Quantachrome. The samples were previously outgassed at 150 °C. The Brunauer–Emmett–Teller (BET) equation was used to determine the specific area using the values of the adsorbed volume between relative pressures P/P_0 of 0.05 to 0.3. The Barret–Joyner–Halenda (BJH) method was used to determine the pore volume (Vp) and pore diameter (DTP). Vp was determined from the amount of gas adsorbed at a relative pressure close to unity.

The conductivity measurements were performed at room temperature in a two-electrode cell with an SS|sample|SS configuration. A 150 mg support sample was compacted to form a wafer that was placed between two electrodes with a cross-sectional area (A) of 1.76 cm^2. The AC impedance spectrum was collected in a frequency range from 1 MHz to 0.1 Hz with a rms amplitude of 10 mV to determine the ohmic resistance (R). The conductivity (σ) was calculated with the following equation:

$$\sigma = \frac{1}{p} = \frac{l}{RA} \qquad (1)$$

where l is the distance between electrodes (wafer thickness) in cm [22].

The total acidity (TA) and the maximum acid strength (MAS) of the support surface sites were determined by potentiometric titration with n-butylamine (NBTA). First, 0.15 g of support was dispersed in 50 mL of acetonitrile (HPLC grade). Then, 0.2 mL of a 0.025 M n-butylamine solution was added to the system, which was left under vigorous stirring for 3 h. Subsequently, 0.2 mL of the same 0.025 M n-butylamine solution was added every two minutes. The potential variation was monitored using a Ag/AgCl electrode and a digital potentiometer. The TA is represented by the potential range in which a plateau is reached and is represented in meq NBTA g^{-1}. The initial electrode potential represents the MAS and was assigned according to the following potential ranges: E > 100 mV very strong site; 0 < E < 100 mV strong site; -100 < E < 0 mV weak site; and E < -100 mV very weak site [23]. The tritrations were performed at 25 °C.

2.4 Electrochemical characterization

Cyclic voltammetry (CV) experiments were carried out in a three-electrode cell at 25 °C. A mercury-mercurous sulfate (Hg/Hg_2SO_4) electrode was used as a reference, and a graphite rod was used as the auxiliary electrode. Each of the prepared materials was studied as a working electrode. For this study, we prepared a catalytic ink by dispersing each milligram of the catalyst in 10 µL of Nafion at 5% weight and 10 µL of 2-propanol in an ultrasonic bath for 20 minutes. Subsequently, 3 µL of this ink was deposited on a glassy carbon disk electrode with a diameter of 5 mm. We used a 0.5 M H_2SO_4

solution as the supporting electrolyte and a 1.0 M CH_3CH_2OH + 0.5 M H_2SO_4 solution as the working medium. The voltammograms were obtained with a potentiostat/galvanostat equipped with a FRA module. The reported potentials are referenced to the Normal Hydrogen Electrode (NHE). Before performing the CV experiment, the working electrodes were stabilized by potential cycling in the 0 to 1 V potential range with a scan rate of 100 mVs^{-1} in 0.5 M H_2SO_4. This process was repeated until no changes in the current density were observed. The catalytically active area was calculated from the electrical charge of the proton adsorption-desorption region in the cyclic voltammogram obtained in the supporting electrolyte at 50 mVs^{-1}. A charge of 0.210 $mCcm^{-2}$ was used as a reference. The catalytic area was also calculated by determining the limiting capacitance. As a reference, a capacitance of 0.195 mF was considered to correspond to 1 cm^2 of Pt surface [24]. The limiting capacitance values were obtained with electrochemical impedance spectroscopy (EIS) measurements at 0.3 V vs. NHE with a frequency sweep from 10 kHz to 0.1 Hz and an amplitude of 5 mV. CV experiments in the working medium with ethanol were performed in 0 to 1.5 V potential range with a scan rate of 10 mVs^{-1}. The sweep was performed in the direction toward positive potentials. The charge transfer resistance (Rct (Ω)) was determined by EIS characterizations performed in the working medium with a scan frequency range of 10 kHz to 0.01 Hz with an amplitude of 5 mV at, 0.5 V.

3. RESULTS AND DISCUSSION

3.1 Physicochemical characterization of supports

X-ray diffraction analyses were performed to determine the effects on the carbon support structure from the incorporation of titania or zirconia.

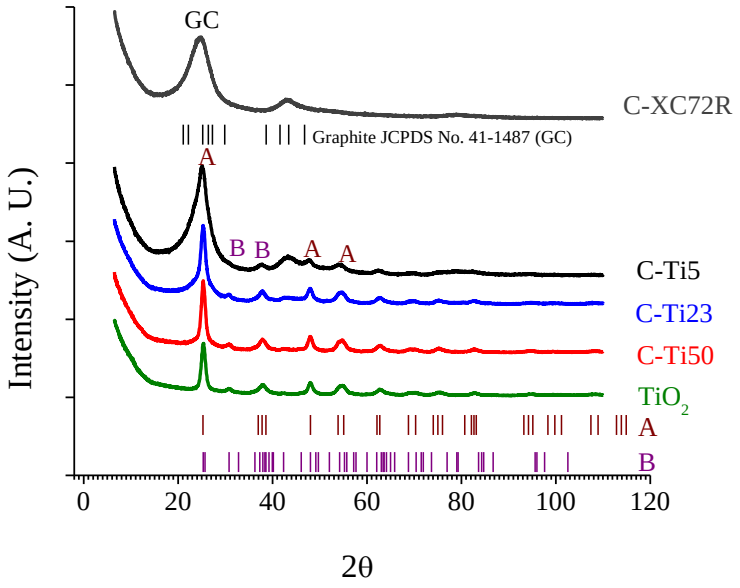

Figure 1. X-ray diffractograms obtained for the C-TiX series calcined at 450 ºC. **A** anatase, **B** brookite, **GC** graphite.

Figure 1 shows the X-ray diffractograms obtained for the C-TiX series and compares them with the reflections of the anatase and brookite phases of TiO_2 (JCPDS No. 21-1272 and 29-1360, respectively) and graphite carbon (JCPDS No. 41-1487). The Vulcan XC72R carbon showed a diffraction peak at approximately $2\theta = 25°$, corresponding to the hexagonal structure of the carbon, as compared to the graphite card. Titanium oxide showed the characteristic peak of the anatase phase at $2\theta = 25.28°$, and in the diffractograms of all the C-TiX composites, this peak overlapped that of the carbon. This peak widened as the metal oxide content decreased. The TiO_2 sample and the C-TiX series showed the characteristic reflections of the anatase and brookite crystalline phases due to the calcination temperature used in the sample preparation procedure. It has been reported that titanium dioxide samples calcinated below 400 ºC exhibit only diffraction lines of the anatase phase, but at temperatures equal to or greater than 400 ºC this crystalline phase starts to transform into rutile, which is a thermodynamically more stable phase [25].

Figure 2 shows the X-ray diffractograms obtained for the C-ZrX series and compares them with the reflections of the orthorhombic (JCPDS No. 34-1084), cubic (JCPDS No. 491642), tetragonal (JCPDS No. 42-1164) and monoclinic (JCPDS No. 37-1484) phases of zirconium oxide and carbon (JCPDS No. 41-1487). The ZrO_2 and the C-ZrX series samples exhibited mixtures of tetragonal and monoclinic crystalline phases, similar to those reported by Rossignol [26] for samples calcined at temperatures below 600 °C.

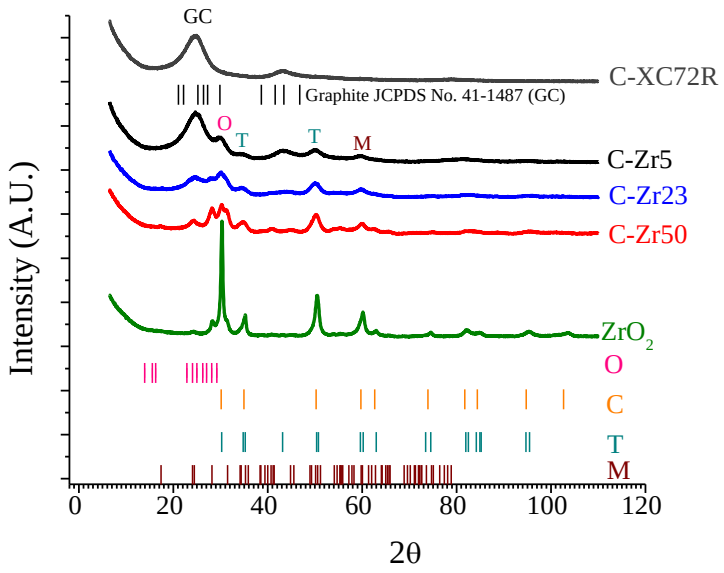

Figure 2. X-ray diffractograms obtained for the C-ZrX series calcined at 450 ºC. **M** monoclinic, **T** tetragonal, **O** orthorhombic, **C** cubic, and **GC** graphite.

The crystallographic cell parameters of the C-TiX and C-Zr composites were determined from the diffractograms. We calculated the average crystal size by using the Scherrer equation. The parameter values are given in Tables 1 and 2. For the C-TiX series, the anatase crystallite sizes were

smaller than that of pure oxide (TiO_2) and ranged from 3.3 to 6.9 nm. It has been reported that the anatase structure is thermodynamically more stable when the crystal size is smaller than 14 nm [27, 28]. For the C-ZrX series, the average crystal size ranged from 2.9 to 41.3 nm.

Table 1 shows that parameter **a** of the carbon cell remained almost constant, while parameter **c** increased slightly with higher TiO_2 contents. There was no significant variation in the cell volume, and the parameter values were similar to those of carbon alone. Because the ionic radius of Ti^{4+} is larger than that of C^{4+} (Ti^{4+} = 0.68 and C^{4+} = 0.15), the cell volume would have increased if Ti^{4+} had been incorporated into the carbon network. We can therefore conclude that the TiO_2 was not introduced into the carbon network. The three C-TiX samples showed the anatase phase. The brookite phase was also present in the C-Ti23 and C-Ti50 samples (Table 2). The crystallite size of the anatase phase increased when the TiO_2 content increased, while the crystallite size of the brookite phase showed the opposite behavior.

Table 1. Carbon lattice parameters, average crystallite size and volume of carbon.

Support	**Carbon Lattice Parameters**		**Carbon Crystallite Size (nm)**	**Volume of Carbon Cell (nm^3)**
	a (nm)	**c (nm)**		
C-XC72R	0.2533(4)	0.7403(4)	0.587(4)	0.0411
C-Ti5	0.2548(3)	0.7674(7)	0.485(3)	0.0431
C-Ti23	0.2509(5)	0.7680(6)	0.425(4)	0.0419
C-Ti50	0.2711(3)	0.8034(6)	0.456(2)	0.0511
C-Zr5	0.2545(6)	0.7429(6)	0.856(5)	0.0417
C-Zr23	0.2646(2)	0.7222(8)	0.402(4)	0.0438
C-Zr50	0.2683(8)	0.7015(8)	0.445(6)	0.0437

For the C-ZrX series, parameters **a** and **c** of the carbon cell remained almost constant. Because the ion radius of Zr^{4+} is higher than that of C^{4+} (Zr^{4+} = 0.80 and C^{4+} = 0.15), the cell volume would increase if Zr^{4+} was incorporated into the carbon network; otherwise, the carbon cell volume would remain relatively unchanged. Thus, the ZrO_2 was not incorporated into the carbon network. The three samples showed the orthorhombic phase, and the C-Zr23 and C-Zr50 samples exhibited the baddeleyite phase as well. C-Zr23 showed the largest crystallite size for the orthorhombic phase, and the crystallite size of baddeleyite phase increased as the ZrO_2 content increased.

Table 2. Titania polymorphs and zirconia polymorph lattice parameters and crystallite sizes.

Support	**Lattice Parameters (nm)**						**Crystallite Size (nm)**	
C-TiX Series	Anatase			Brookite				
	a		**c**	**a**	**b**	**c**	Anatase	Brookite
C-Ti5	0.3859(3)		1.0715(8)	---	---	---	3.258(5)	---
C-Ti23	0.3837(2)		1.0723(9)	0.9379(6)	0.5477(3)	0.5253(8)	6.874(5)	6.236(4)
C-Ti50	0.3829(2)		1.0727(5)	0.9355(8)	0.5494(3)	0.5409(6)	11.621(4)	3.056(7)
C-ZrX Series	Orthorhombic			Baddeleyite				
	a	**b**	**c**	**a**	**b**	**c**	Orthorhombic	Baddeleyite
C-Zr5	0.5129(2)	0.5299(1)	0.5316(3)	---	---	---	2.877(2)	---
C-Zr23	0.5244(3)	0.5165(2)	0.5148(6)	0.5156(2)	0.5352(4)	0.5423(5)	41.262(2)	2.768(3)
C-Zr50	0.5192(3)	0.5158(2)	0.5113(3)	0.5179(6)	0.5287(9)	0.5317(2)	38.776(3)	5.321(4)

Table 3 shows the contents of the crystalline phases present in weight percentage. For the C-TiX series, the brookite phase was present in a higher proportion. For the C-ZrX materials, the predominant phase was orthorhombic; however, as the metallic content increased, a more significant amount of the baddeleyite phase was observed.

Table 3. Weight percent of carbon-titania polymorphs and carbon-zirconia polymorphs.

Support	**Wt (%)**				
	Carbon	**Anatase**	**Brookite**	**Orthorhombic Zirconia**	**Baddeleyite**
C-Ti5	85.1	14.9			
C-Ti23	69.72	6.83	23.45		
C-Ti50	77.6	7.14	15.26		
C-Zr5	69.39			30.61	
C-Zr23	53.33			37.97	8.7
C-Zr50	49.06			38.04	12.9

The textural properties of the supports were determined from nitrogen physisorption experiments at 77 K. The specific area, pore volume and average pore size obtained for the different materials are presented in Table 4. The pure oxides, TiO_2 and ZrO_2, had smaller specific areas than the Vulcan XC72R carbon and the composite supports. In the C-TiX series, the specific area decreased as the TiO_2 content increased. In the C-ZrX series, the C-Zr50 sample had the highest area and pore volume, followed by the C-Zr5 sample, probably due to the presence of amorphous remnants of Zr hydroxides. The C-Zr23 sample had the smallest area and the lowest pore volume. In the C-ZrX series, the pore diameter decreased as the ZrO_2 content increased.

Table 4. Physicochemical properties of the C-TiX and C-ZrX supports: textural properties (BET area, pore volume, and pore diameter), conductivity, bandgap (Eg) and surface acidity.

Support	BET area (m^2/g)	Pore volume (mL/g)	Pore diameter (Å)	σ ($S\ cm^{-1}$)	Eg (eV)	MAS* (mV)	TA** (meq NBTA g^{-1})
C-XC72R	311	0.716	164	0.4	1.3	151	27
C-Ti5	277	1.084	269	0.8	1.8	111	34
C-Ti23	228	0.902	249	0.4	3.3	122	37
C-Ti50	160	0.794	221	0.3	3.7	130	37
TiO_2	118	0.432	99	$1.4x10^{-0.5}$	3.3	97	32
C-Zr5	151	0.074	224	0.6	2.0	126	44
C-Zr23	115	0.554	194	0.4	3.7	60	41
C-Zr50	264	0.690	180	0.1	4.5	40	34
ZrO_2	66	0.228	137	$2.2x10^{-0.5}$	5.5	43	39

*MAS=Maximum acid strength, **TA=Total acidity

For both the C-TiX and C-ZrX series, the support conductivity was higher at lower oxide loadings in the formulations, which was consistent with the lower bandgap values (Table 4) that were due to the semiconducting nature of TiO_2 and ZrO_2. The C-Ti5 sample had a bandgap of 1.8 eV and a conductivity of 0.8 Scm^{-1}, while the C-Ti50 support had a higher bandgap of 3.7 eV and lower conductivity of 0.3 S cm^{-1}. However, these conductivity values were higher than those for pure TiO_2 oxide, which had a conductivity of 1.4 x $10^{-0.5}$ Scm^{-1} and a bandgap of 3.3 eV. The TiO_2 bandgap obtained in this work agrees with that reported in [29, 30]. Similarly, for the C-ZrX series, the C-Zr5 sample had a bandgap of 0.4 eV and a conductivity of 0.6 Scm^{-1}, and the C-Zr50 sample had a higher bandgap of 4.5 eV and a lower conductivity of 0.1 Scm^{-1}. The ZrO_2 support showed the lowest conductivity of the series, which was 2.2 x $10^{-0.5}$ Scm^{-1}, and had a bandgap of 5.5 eV, which is similar to what was reported in [31]. Thus, the incorporation of TiO_2 and ZrO_2 into carbon modified its electronic properties. The differences in the bandgap values (Table 4), which are influenced by the composition of the support, may also be due to the crystal sizes (Table 1) [32].

N-butylamine titrations were performed to evaluate the surface acidity properties of the synthesized supports. Figure 3a shows that the incorporation of TiO_2 improved the surface acidity of all the C-TiX composites. The maximum acid strength (MAS) increased with increasing TiO_2 loading (Table 4). The carbon exhibited a very strong acid strength of 151 mV, which was higher than the acid strength of all the composite supports. However, the total acidity (TA) of the C-TiX composites was higher than that of the carbon support. According to the classification scheme for acidity strength reported by Pizzio [23], all the composite supports showed an MAS equivalent to very strong acid sites except the pure TiO_2 support, which exhibited a value of 97 mV at the limit between strong and very strong sites.

In contrast, in the C-ZrX series (Figure 3b), the acid strength decreased as the zirconium content in the support increased, with values of 126, 60 and 40 mV for the C-Zr5, C-Zr23 and C-Zr50 samples, respectively. The same behavior was observed for the acid site concentration (meq NBTA g^{-}

[1]). The C-Zr5 sample, with the lowest zirconium loading, showed a surface acid strength close to that of the carbon support, while the rest of the materials in the C-ZrX series had values close to that of the pure zirconia support. The TiO_2 concentration on the surface was more favored than that of ZrO_2, given that there was almost no variation in the total acidity values in the C-TiX series, while in the C-ZrX series there were significant changes.

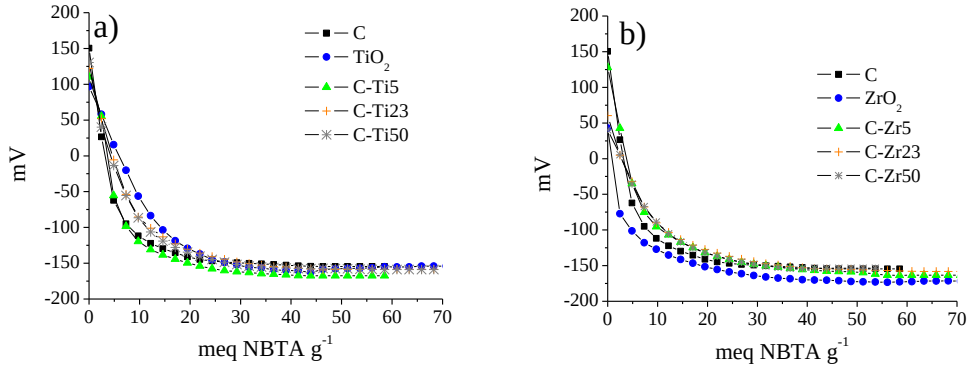

Figure 3. Potentiometric titration of the series: a) C-TiX and b) C-ZrX. T= 25 °C.

3.2 Electrochemical characterization of the catalysts

Figure 4a shows the voltammograms of the Pt/C and Pt/C-TiX series recorded at a scan rate of 50 mVs^{-1} in a potential window from 0 to 1.5 V. For the Pt/C catalyst, three peaks associated with the desorption of protons are shown at 0.04, 0.09 and 0.16 V in the scan toward positive potentials [33]. The signal at 0.5 V is attributed to the oxidation of the functional groups of the support [34]. The oxidation of Pt^0 to Pt^{2+} started at 0.7 V. Finally, the oxygen evolution reaction began at 1.3 V. On the return scan, toward negative potentials, Pt was reduced from Pt^{2+} to Pt^0. The reduction started at 0.9 V, and reached a maximum at 0.65 V. Proton adsorption was observed at approximately 0.15 V. Finally, hydrogen evolution was observed at potentials close to 0 V. For the Pt/C-TiX series, the current and active area increased with the TiO_2 content of the support. The active areas were 1.4, 3.3 and 3.8 m^2g^{-1} for Pt/C-Ti5, Pt/C-Ti23 and Pt/C-Ti50, respectively (Table 5). In contrast, in the Pt/C-ZrX series (Figure 4b), the current decreased with the ZrO_2 content. The Pt/C-Zr50 catalyst had the smallest active area, which was 0.4 m^2g^{-1}, followed by Pt/C with a value of 2.9 m^2g^{-1}. Pt/C-Zr5 and Pt/C-Zr23 had higher active areas of 4 and 3 m^2g^{-1}, respectively. Similar active area values were obtained by determining the limiting capacitance via electrochemical impedance spectroscopy (Table 5) [24].

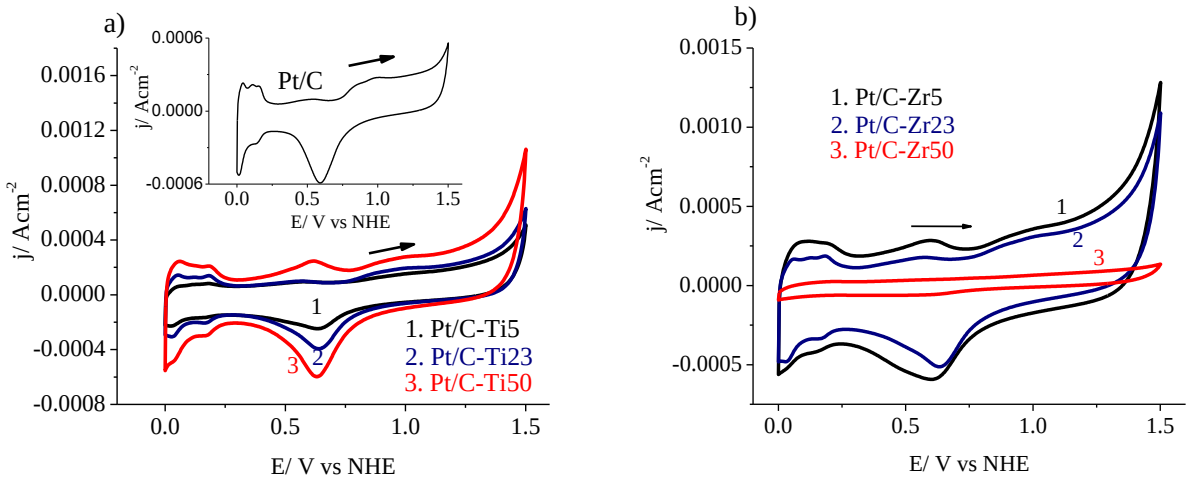

Figure 4. CV of the catalyst series: a) Pt/C-TiX and b) Pt/C-ZrX in 0.5 M H_2SO_4, from 0 to 1.5 V vs. NHE at a scan rate of 50 mV s^{-1}, and T= 25 °C.

Figures 5a and 5b show the voltammograms for the Pt/C-TiX and Pt/C-ZrX series obtained in the working medium at a sweep rate of 10 mV s^{-1}. All the voltammograms were normalized with respect to the catalytically active area (Table 5) [1]. Three oxidation peaks are present. In the sweep toward positive potentials, there are two peaks related to the formation of intermediate species: the first peak is due to the oxidation of ethanol to acetaldehyde (peak A), and the second peak corresponds to the formation of acetic acid (peak B). The oxidation peak recorded in the return sweep toward negative potentials (peak C) corresponds to the oxidation of the intermediate species adsorbed on the catalyst surface promoted by the reduction of Pt^{2+} to Pt^0.

For the Pt/C-TiX series (Figure 5a), the following trend in current density was observed: Pt/C > Pt/C-Ti5 > Pt/C-Ti50 > Pt/C-Ti23. With the incorporation of TiO_2 into the support, the first two peaks (A and B) registered a shift toward negative potentials of approximately 0.1 V (Table 5). Less energy was needed to initiate the ethanol electro-oxidation process. For Pt/C, the starting potential was 0.43 V, while for the Pt/C-Ti-5, Pt/C-Ti23 and Pt/C-Ti50 catalysts it was recorded at 0.36, 0.30 and 0.34 V, respectively. Likewise, there was a shift to lower values for the main peak potentials of the two peaks A and B. For the Pt/C these peaks were recorded at 0.9 V and 1.25 V. For the Pt/C-Ti5, Pt/C-Ti23 and Pt/C-Ti50 catalysts, the current maxima for peak A were recorded at 0.83, 0.82 and 0.85 V, respectively; for peak B at 1.20, 1.20 and 1.21 V, respectively. For the Pt/C-ZrX series (Figure 5b), the current density behavior was as follows: Pt/C > Pt/C-Zr5 > Pt/C-Zr23 > Pt/C-Zr50. Similar to the observations for the catalysts containing TiO_2, the presence of ZrO_2 in the support favored a shift toward negative potentials in the onset potential and the potential in which the maxima of peaks A and B appeared. The starting potential was recorded at 0.42, 0.35 and 0.35 V for the Pt/C-Zr5, Pt/C-Zr23 and Pt/C-Zr50 catalysts, respectively. The main peak potential of peak A was present at 0.85, 0.83 and 0.85 V and for peak B at 1.20, 1.20 and 1.26 V for the Pt/C-Zr5, Pt/C-Zr23 and Pt/C-Zr50 catalysts, respectively. These trends agree with the total acidity results, demonstrating the participation of the surface acid sites in the electro-oxidation of ethanol, possibly through the weakening of the C–C bond.

Greater shifts toward negative potentials were observed with the Pt/C-TiX series than with the Pt/C-ZrX series. This trend may be due to the greater acid strength of the materials modified with TiO_2.

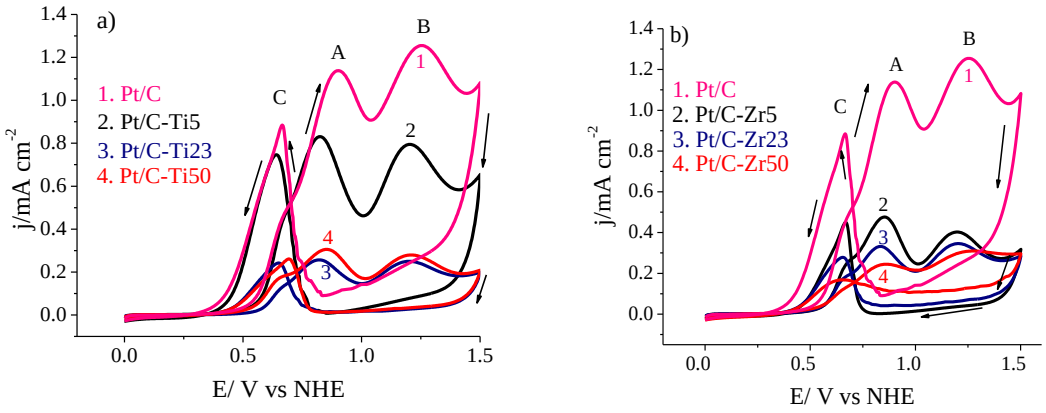

Figure 5. CV of a) Pt/C-TiX and b) Pt/C-ZrX series in working medium (0.5 M H_2SO_4 + 1.0 M CH_3CH_2OH) from 0 to 1.5 V at 10 mVs^{-1}, and T= 25 °C.

Electrochemical impedance spectroscopy analyses of the Pt/C-TiX and Pt/C-ZrX series in the working medium were performed at 0.5 V, the region in which the intermediate species began to form (Figure 6) [35]. To compare the electrochemical activity of the different catalysts, the charge transfer resistance was calculated by fitting the data from the complex impedance plane plots to the equivalent circuit shown in Figure 7.

Table 5. Electrochemical results of cyclic voltammetry, electroactive area, and R_{CT} for Pt/C-TiX and Pt/C-ZrX series.

Catalyst	Peak A			Peak B		Peak C		Electroactive area m^2g-1		EIS
	E_{Onset} V*	i max $mAcm^{-2}$	$E_{i\ max}$ V*	i max $mAcm^{-2}$	$E_{i\ max}$ V*	i max $mAcm^{-2}$	$E_{i\ max}$ V*	Determined by CV	Determined By IES	R_{CT} Ω
Pt/C	0.43	1.14	0.90	1.25	1.25	0.88	0.67	2.9	2.8	2250
Pt/C-Ti5	0.36	0.83	0.83	0.79	1.20	0.75	0.64	1.4	1.4	2550
Pt/C-Ti23	0.30	0.26	0.82	0.26	1.20	0.24	0.65	3.3	3.4	1675
Pt/C-Ti50	0.34	0.30	0.85	0.28	1.21	0.26	0.69	3.8	3.7	5980
Pt/C-Zr5	0.42	0.48	0.85	0.40	1.20	0.45	0.67	4.0	4.2	3980
Pt/C-Zr23	0.35	0.33	0.83	0.35	1.20	0.28	0.65	3.0	3.1	2252
Pt/C-Zr50	0.35	0.24	0.85	0.31	1.26	0.17	0.65	0.4	0.3	8300

*V vs NHE

This circuit consisted of a resistance associated with the electrolyte and the ohmic losses (Rs) that are found in series with a parallel arrangement of a constant phase element (CPE), which represents a double layer capacitance, and a resistance related to the charge transfer at the electrode-electrolyte interface (R_{CT} (Ω)). For the Pt/C-TiX series, the Pt/C-Ti23 material exhibited a smaller diameter semicircle at 0.5 V, which implies a lower Rct and greater activity, followed by the Pt/C-Ti5 and Pt/C materials, and finally Pt/C-Ti50, which was the least active. For the Pt/C-ZrX series, the activity for the ethanol electro-oxidation reaction exhibited the following trend: Pt/C-Zr23 > Pt/C > Pt/C-Zr5 > Pt/C-Zr50. The Pt/C-TiX series had lower Rct values than did the Pt/C-ZrX series. These results agree with the CV and acidity results.

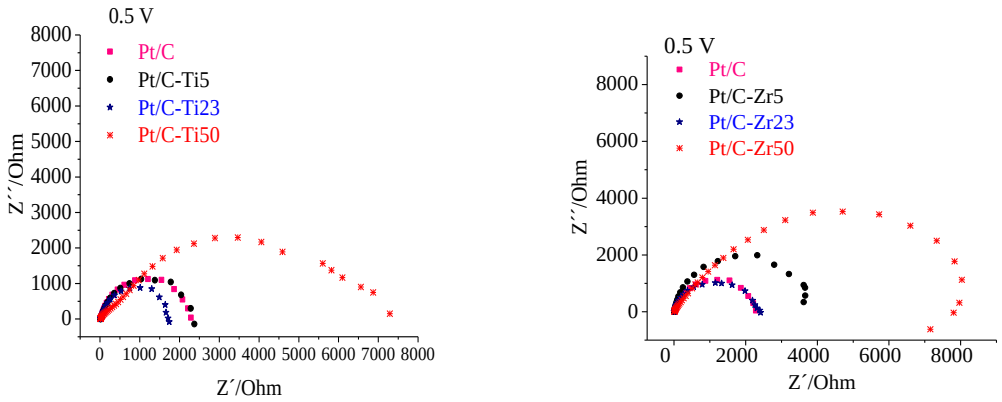

Figure 6. EIS plots of a) Pt/C-TiX and b) Pt/C-ZrX series at 0.5 V vs. NHE in working solution (0.5 M H_2SO_4 + 1.0 M CH_3CH_2OH) at 10 mVs^{-1}, and T= 25 °C.

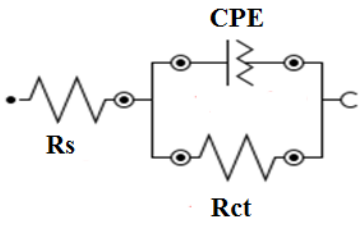

Figure 7. Equivalent circuit for the synthesized catalysts

4. CONCLUSIONS

The carbon composite materials studied (C-TiO_2 and C-ZrO_2) showed mesoporous characteristics. The XRD results for the C-TiX and C-ZrX series indicated that TiO_2 and ZrO_2 remained segregated on the carbon surface, as no changes were observed in the properties of the carbon network. The conductivities of the supports were reduced with the incorporation of TiO_2 and ZrO_2; however, the presence of these oxides favored the formation of more acid sites compared to those of the carbon support. According to the onset potential and the Rct, the presence of TiO_2 and ZrO_2 in the support modified the activity of the Pt catalyst either through the presence of OH^- groups

on the surface or by weakening the C–C bond due to the presence of a higher concentration of acid sites. However, to have higher activity, there must be a balance between the surface acidity provided by the metal oxide content and the conductivity of the support. In both series, the sample with a metal oxide loading of 23 wt% showed higher activity. The XRD results treated with the Rietveld method and electrochemical results, demonstrated that in the C-TiX series, the brookite phase promotes a higher catalytic activity for the oxidation of ethanol. In the C-ZrX series, the orthorhombic phase exhibited better catalytic activity. Comparing the catalytic performances of the two series, the catalysts supported on C-TiO_2 exhibited more significant catalytic activity than did the catalysts supported on C-ZrO_2, since the former had a greater acid strength.

ACKNOWLEDGMENTS
The authors thank the financial support of the CONACYT-SENER-Sustentabilidad Energética-LENERSE project No. 254667. Marisol Castro thanks CONACYT for the 221950 scholarship. The Authors thank M. C. José Martín Baas for the N_2 physisorption tests and M.C. Enrique Escobedo for the technical assistance in the electrochemistry laboratory of Renewable Energy Department.

References

1. C. Lamy, E.M. Belgsir and J.M. Léger, *J. App. Electrochem.*, 31 (2001) 799.
2. A. Bauer, C. Song, A. Ignaszak, R. Hui, J. Zhang, L. Chevallier, D. Jones, and J. Rozière, *Electrochim. Acta*, 55 (2010) 8365.
3. L.G.S. Pereira, F.R. Dos Santos, M.E. Pereira, V.A. Paganin and E.A. Ticianelli, *Electrochim. Acta*, 51(2006) 4061.
4. N. Laidani, V. Micheli and M. Anderle, *Thin Solid Films*, 382 (2001) 23.
5. Y. Bai, J. Wu, J. Xi, J. Wang, W. Zhu, L. Chen and X. Qiu, *Electrochem. Commun.*, 7(2005) 1087.
6. P.J. Kulesza, I.S. Pieta, I.A. Rutkowska, A. Wadas, D. Marks, K. Klak, L. Stobinski and J.A. Cox, *Electrochim. Acta*, 110 (2013) 474.
7. B. Ruiz-Camacho, J.H. Martínez-González, R.G. González-Huerta and M. Tufiño-Velázquez, *Int. J. Hydrogen Energ.*, 39 (2014) 1673.
8. Z. Wang, G. Chen, D. Xia and L. Zhang, *J. Alloy Compd.* 450 (2008) 148.
9. J. Tian, G. Sun, L. Jiang, S. Yan, Q. Mao and Q. Xin, *Electrochem. Commun.* 9 (2007) 563.
10. N. Chaisubanan, K. Pruksathorn, H. Vergnes, F. Senocq and M. Hunsom, *Int. J. Electrochem. Sci.* 11(2016) 1012.
11. N. Kitiphatpiboon and M. Hunson, *Int. J. Electrochem. Sci.* 11(2016) 2741.
12. S. Von Kraemer, K. Wikander, G. Lindbergh, A. Lundblad and A.E.C. Palmqvist, *J. Power Sources,* 180 (2008) 185.
13. J. Shim, C. R. Lee, H.K. Lee, J.S. Lee and E.J. Cairns, *J. Power Sources* 102 (2001) 172.
14. L. Xiong, and A. Manthiram, *Electrochim. Acta*, 49 (2004) 4163.
15. H. Song, X. Qiu, and F. Li, *App. Catal. A-Gen.*, 364 (2009) 1.
16. D.J. Guo, X.P. Qiu, W.T. Zhu and L.Q. Chen, *Appl. Catal. B- Environ.*, 89 (2009) 597.
17. R. Vinodh, M. Purushothaman, and D. Sangeetha, *Int. J. Hydrogen Energ.*, 36 (2011) 7291.
18. A. Coelho, Academic V4.1, Coelho Software Brisbane, Australia; web site: www.topas-academic.net.
19. M. Järvinen, *J. Appl. Cryst.*, 26 (1993) 525.
20. P.W. Stephens, *J. Appl. Cryst.*, 32 (1999) 281.

21. E. Prince, *J. Appl. Cryst.*, 14 (1981) 157.
22. F. López-García, G. Canché-Escamilla, A.L. Ocampo-Flores, P. Roquero-Tejeda, L.C. Ordóñez, *Int. J. Electrochem. Sci.*, 8 (2013) 3794.
23. L.R. Pizzio, P.G. Vázquez, C.V. Cáceres and M.N. Blanco, *Appl. Catal. A-Gen.*, 256 (2003) 125.
24. E.B. Easton, P.G. Pickup, *Electrochim. Acta,* 50 (2005) 2469.
25. S.R. Yoganarasimhan and C.N.R. Rao, *T. Faraday Soc.*, 58 (1962) 1579.
26. S. Rossignol, Y. Madier. *Catal. Today*, 50 (1999) 261.
27. M.R. Ranade, A. Navrotsky, H.Z. Zhang, J.F. Banfield, S.H. Elder, A. Zaban, P.H. Borse, S.K. Kulkarni, G.S. Doran and H.J. Whitfield. *Proc. Natl. Acad. Sci. USA,* 99 (2002) 6476.
28. H. Zhang and J.F. Banfield, *J. Mater. Res.*, 15 (2000) 437.
29. S.S. Valencia, J.M. Marín and G. Restrepo, *Open Materials Science Journal*, 4 (2009) 9.
30. X. Zhang, Y. Sun, X. Cui and Z. Jiang, *Int. J. Hydrogen Energ.* 37 (2012) 1356.
31. S.M. Chang and R.A. Doong, *Chem. Mater.*, 19 (2007) 4804.
32. M.C. Hidalgo, M. Aguilar, M. Maicu, J.A. Navío and G. Colón, *Catal. Today*,129 (2007) 50.
33. N.M. Marković, B.N. Grgur and P.N. Ross, *J. Phys. Chem. B.*, 101 (1997) 5405.
34. J.L. Figueiredo, M.F.R. Pereira, M.M.A. Freitas and J.J.M. Órfão, *Carbon*, 37 (1999) 1379.
35. S. S. Gupta and J. Datta, *J. Chem. Sci.*, 117 (2005) 337.